IET Systems Biology

Research Article

IET Journals
The Institution of Engineering and Technology

Coupling of cell fate selection model enhances DNA damage response and may underlie BE phenomenon

ISSN 1751-8849
Received on 6th August 2019
Revised 24th September 2019
Accepted on 31st October 2019
E-First on 30th January 2020
doi: 10.1049/iet-syb.2019.0081
www.ietdl.org

Gökhan Demirkıran[1] ✉, Güleser Kalaycı Demir[2], Cüneyt Güzeliş[1]

[1]*Electrical and Electronics Engineering, Yaşar University, Selçuk Yaşar Kampüsü, İzmir, Turkey*
[2]*Electrical and Electronics Engineering, Dokuz Eylül University, Tınaztepe, İzmir, Turkey*
✉ *E-mail: gokhan.demirkiran@yasar.edu.tr*

Abstract: Double-strand break-induced (DSB) cells send signal that induces DSBs in neighbour cells, resulting in the interaction among cells sharing the same medium. Since p53 network gives oscillatory response to DSBs, such interaction among cells could be modelled as an excitatory coupling of p53 network oscillators. This study proposes a plausible coupling model of three-mode two-dimensional oscillators, which models the p53-mediated cell fate selection in globally coupled DSB-induced cells. The coupled model consists of ATM and Wip1 proteins as variables. The coupling mechanism is realised through ATM variable via a mean-field modelling the bystander signal in the intercellular medium. Investigation of the model reveals that the coupling generates more sensitive DNA damage response by affecting cell fate selection. Additionally, the authors search for the cause-effect relationship between coupled p53 network oscillators and bystander effect (BE) endpoints. For this, they search for the possible values of uncertain parameters that may replicate BE experiments' results. At certain parametric regions, there is a correlation between the outcomes of cell fate and endpoints of BE, suggesting that the intercellular coupling of p53 network may manifest itself as the form of observed BEs.

1 Introduction

Biological endpoints observed in a group of irradiated cells differ when that group interacts with another group that is irradiated at a different dose. This phenomenon is broadly called the bystander effect (BE), which has been categorised into Type-1, Type-2, Type-3 and rescue effect. Type-1, widely referred as radiation-induced BE in several studies can be described as the decreased cell survival and the formation of DNA damage in unirradiated (non-targeted) cells neighbouring irradiated (targeted) cells [1]. Type-2 effect is the increased cell survival in the low-irradiated group of cells neighbouring high-irradiated group of cells, whilst Type-3 effect is the increased cell survival in high-irradiated group of cells neighbouring low-irradiated group of cells [2]. Additionally, Chen *et al.* [3] showed the positive influences such as the increase in cell survival rates and the decrease in the number of double-strand breaks (DSBs), in irradiated cells neighbouring unirradiated (no-dose applied) cells, which they call as 'rescue effect'. Rescue effect differs from Type-3 in the sense that rescue effect occurs between unirradiated and irradiated cells whilst Type-3 occurs between low-irradiated and high-irradiated cells.

Although BE has been observed and demonstrated at the phenomenological level at several studies [1], its underlying mechanism is not completely understood, which poses obstacles to finding protocols in radiotherapy that benefit from BE phenomenon [4]. Since BE (Type-1) has been implicated in low-dose hyper radio-sensitivity (HRS) and increased radio resistance (IRR) [5] that are of clinical importance [6, 7], several computational studies that are done in the context of BE pay special attention to the understanding of HRS/IRR. For instance, Peng *et al.* [8] introduce bystander terms into linear quadratic radiobiological formulation to better fit cell survival data. Powathil *et al.* [9] include cell cycle phase information of non-targeted (bystander) and targeted cells to predict cell survivals. Powathil *et al.* [10] propose a multiscale model incorporating spatiotemporal information of bystander, oxygen distribution and cell cycle phases. Cell cycle dynamics in BE signalling also has been studied by Hattori *et al.* [11] via cellular automaton-based model. The integrated microdosimetric-kinetic model has been proposed to reveal the role of DNA repair kinetics in HRS [12].

There are a variety of models validated by experimental data, which aims to understand HRS/IRR and bystander signalling dynamics to revise strategies in radiotherapy. However, all the mentioned *in-silico* studies focus on the process of Type-1 behaviour. To our knowledge, there is no *in-silico* study on Type-2 or Type-3 behaviour. Thus, the questions such as 'How BE results in enhanced cell survival as in Type-2 or Type-3?' and 'What are the mechanisms underlying such counter-intuitive results?' remain as challenging questions that need to be elucidated. That being said, the aim of this paper is to give a mathematical framework explaining the underlying mechanism of BEs and to reveal how irradiated cells benefit. Further than that, our interest is to unify Type-1, Type-2 and Type-3 behaviours in one unifying model that gives system-level insights.

Studies suggest that communication signal of BE among cells mostly relies on DSB formation induced by radiation rather than other induced base damages [13–15] and that DSB formation is accepted as the upstream event that leads to BE [16]. DSBs are the highly deleterious type of DNA damage that is responded via oscillatory p53 network response [17, 18]; thus, DSB induction appears to be a stimulus for both oscillatory p53 network and BE phenomenon. Since p53 network is the key regulator of biological endpoints such as DNA repair, cell cycle arrest (CCA) and apoptosis, the evidence for participation of p53 network in BE phenomenon is obtained by showing a correlation between p53 expression levels and those biological endpoints in bystander cells [19]. Additional studies also reveal that p53 network might contribute to the biological endpoints in BE phenomenon by triggering apoptotic response [4, 20] or p53-mediated DNA damage responses on receiving bystander signals [21]. Although considerable amount of papers are devoted to p53 network and BE *in vivo* or *in vitro*, there are limited number of *in-silico* studies that investigate the role of p53 network in BE phenomenon [22, 23]. These *in-silico* studies treat BE signalling among cells as a coupling mechanism that couples oscillatory p53 dynamics of cells, and show the increase in robustness of p53 oscillations via synchronisation. However, an integrating study on how the types of BE may emerge from this coupling behaviour, and what is the benefit of coupling from the vantage point of cell fate selection is missing from the literature.

© The Institution of Engineering and Technology 2019

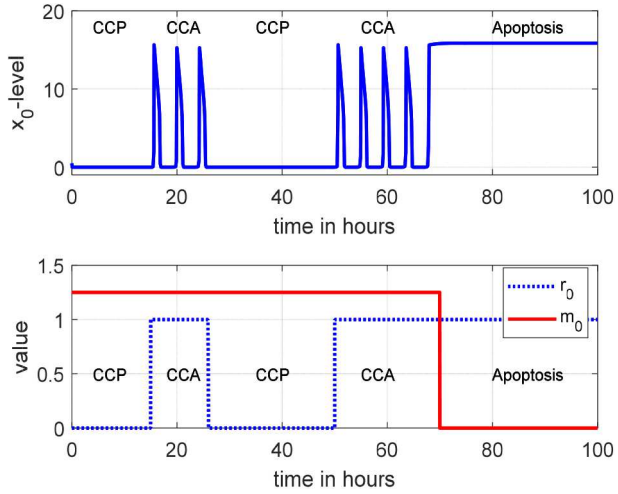


Fig. 1 *Three modes of p53 dynamics controlling cell fate selection via two-phase dynamics in the zeroth reference cell. The fixed parameters of the reference cell are* $a_0 = 5$, $b_0 = 10$, $c_0 = 15$, $d_0 = 70$, $m_{0,\,\text{normal}} = 1.25$, $n_0 = 0.8$, $z_0 = 0.5$, $\tau_{0,\,1} = 1$, $\tau_{0,\,2} = 2$.

(a) x-Level of the reference cell, when, ***(b)*** Tunable mode design parameters $\{r_i, m_i\}$ are $\{0, 1.25\}$, $\{1, 1.25\}$, $\{0, 1.25\}$, $\{1, 1.25\}$, $\{0, 1.25\}$ between time intervals $[0, 15)$, $[15, 26)$, $[26, 50)$, $[50, 66)$, $[66, 100]$, respectively

Studies in biological oscillatory systems have revealed that synchronisation is a form of intercellular information and provides a certain biological function. For example, coupling in circadian clock oscillator confers robustness against genetic heterogeneity among cells [24]. Nuclear factor kappa B (NF-KB) oscillator use noise to help achieve synchronisation and produce more stable oscillations [25] and calcium systems use noise for the transition from stable state to oscillatory state [26]. The information of density of population in Vibrio fischeri can use intercellular coupling mechanisms to transfer information among each other [27]. Coupling in circadian rhythm brings many advantages that increases the fitness of the organism [28, 29]. Here, we emphasise that these examples from the literature focus solely on the oscillation process, which is the only functional operating mode in the studied oscillators. However, in our case, p53 network oscillator has three functional modes: (i) low level of p53 associated with cell cycle progression (CCP), (ii) oscillatory state of p53 associated with CCA and (iii) high level of p53 associated with apoptosis. Thus, a natural question arises as 'What is the role of coupling in coordination of these three modes (i.e. cell fate selection) related to BE?', which has not been studied yet to the best of authors' knowledge.

In this paper, we research with the expectation that the observation of BE phenomenon at the tissue (phenomenological) level can be elevated to the systems level of understanding via investigating the dynamic properties of cell fate selections in cells coupled through their p53 networks. For the cell fate selection in an uncoupled single cell, we use the two-dimensional (2D) oscillator model of p53 dynamics under DSBs by Demirkıran *et al.* [30]. The model is based on the indispensable and most important components leading to oscillatory p53 dynamics (i.e. Ataxia telangiectasia mutated (ATM) and Wip1 interaction [31]). Then, based on the literature on intercellular communication of p53 networks of cells in BE phenomenon, we extend the model by introducing a coupling term for the 2D oscillator model. To make the research workable, and to obtain statistical information on cell fate decisions, we do not include repair mechanics in cells. We further assume that damage signalling, i.e. DSB induction, in the population of cells is immediate, and thus we assume a homogeneous intercellular medium. The resulting coupled model is used as a minimal model for investigating dynamic properties of cell fate selection in coupled cells under DSBs. The analyses on the minimal coupled model reveal that:

- With the introduction of coupling, the distribution of oscillation periods in a group becomes more focused around a smaller mean value, which increases the average p53 level of cells in a fixed interval and decreases the likelihood of exhibiting ineffective long periods.
- More rapid response to DSB is obtained as the coupling strength increases. Thus, the sensitivity toward DNA damage increases.
- Coupled p53 networks of cells replicate the biological endpoints of Type-2 and Type-3 experiments for certain parametric regions, meaning that coupled p53 networks may be the underlying mechanism of BE. We indicate parametric regions that lead to such behaviours.

2 Model description and method

In this section, we propose a minimal coupled model describing p53 dynamics of cells coupled under DSBs, in other words, describing the dynamics of cell fate selection in BE settings. The coupled model is based on a 2D canonical relaxation oscillator model (1) and (2) introduced in [30] by Demirkıran *et al.* to model p53 dynamics controlling cell fate selection under DSBs in a single cell with ID number i and no intercellular interaction. The sets of (1) and (2) can exhibit the three modes of p53 dynamics each corresponding to a certain cellular outcome under relevant condition: low-level mode corresponding to CCP in unstressed conditions, oscillatory mode corresponding to CCA under DSBs and high-level mode corresponding to apoptosis under unrepairable damage. The sets of (1) and (2) are named as the ith cell fate oscillator (CFO), where the parameters of the CFO must obey constraints in (3) and (4) for the ability to exhibit three different modes [30].

The sets of (1) and (2) comprise the bi-stability property of ATM that is denoted with the variable x_i and feedback loop property of Wip1 that is denoted with the variable y_i. It is assumed that p53 dynamics follows ATM dynamics [31]; thus, p53 is not introduced as an additional parameter or variable. Therefore, x_i-dynamics reveals information about cell fate decision in the ith cell. Although there are other biological endpoints involved in BE phenomenon, which are caused by p53 network or other pathways, e.g. senescence by NF-KB pathway [32], in this paper, we will solely focus on p53-mediated DNA damage response and the p53-mediated cell fate outcomes, namely CCA, apoptosis and CCP, under BE settings.

The fixed parameters of (1) and (2) are a_i, b_i, c_i, d_i, $m_{i,\,\text{normal}}$, n_i, z_i, $\tau_{i,\,1}$, and $\tau_{i,\,2}$. There are two tunable model parameters: Wip1 feedback loop strength parameter m_i and damage severity parameter r_i, which jointly determine the operating mode of the oscillator (low level, oscillations or high level); thus, they are named as mode design parameters (Fig. 1). It is assumed that the following conditions are met: $m_i \in [0, m_{i,\,\text{normal}}]$ and $r_i \in [0, 1]$, where $r_i = 0$ indicates no damage, whilst $r_i = 1$ indicates the most difficult situation:

$$\dot{x}_i = \frac{1}{\tau_{i,\,1}}\left(-x_i\left[r_i\left(x_i^2 - (a_i + b_i)x_i\right) + a_i b_i + c_i y_i - r_i d_i\right]\right) \tag{1}$$

$$\dot{y}_i = \frac{1}{\tau_{i,\,2}}(z_i + m_i x_i - n_i y_i)\,. \tag{2}$$

$$a_i b_i - d_i + \frac{c_i z_i}{n_i} < 0 \tag{3}$$

$$\frac{1}{\tau_{i,\,1}}\frac{1}{8}(a_i + b_i)^2 - \frac{1}{\tau_{i,\,2}} n_i > 0 \tag{4}$$

In realistic conditions, a limited number of oscillations – less than few pulses – can be observed due to the following two reasons. First, pro-apoptotic factors accumulate over pulses and alter cell state from oscillations (CCA) to a sustained high level (apoptosis) as they become higher than some threshold. It is suggested that the accumulation to a certain threshold requires 3–4 pulses [33]. Second, DNA repair process may finish the repair, and then alter

© The Institution of Engineering and Technology 2019

the cell state from oscillations (CCA) to low level (CCP) before apoptosis takes place. Thus, sustained high level of p53 shows up only after an oscillation phase, to promote the DSB repair first and then give the ultimate decision of apoptosis if necessary. This behaviour is known as two-phase dynamics of p53 network for cell fate selection, and we will refer to these dynamics for investigating cell fate dynamics in BE settings.

The effect of accumulating pro-apoptotic factors can be embedded via decreasing the parameter m_i with proportional to the time integral of the x_i pulse [34], whilst the repair process can be embedded via decreasing the damage severity parameter r_i according to a model of the repair mechanism [33]. However, this requires at least two additional model variables for every ith cell and complicates the model. Instead, we externally manipulate r_i and m_i parameters directly to have control over cell fate selection for the analysis purposes. For instance, as depicted for the reference cell [the zeroth cell, $i = 0$ in (1) and (2)] in Fig. 1, changing r_0 from 0 to 1 (indicating the induction of DNA damage) with fixing $m_0 = m_{0,\,\text{normal}}$ causes oscillations. Then, decreasing the parameter m_i to a sufficiently low value whilst r_i is still 1 (indicating the long duration of repair) causes a sustained high level [34].

Studies suggest that two mechanisms for the intercellular communication leading to BE exist: (i) gap junctional intercellular communication via transmission of signal from gap junctions in touching cells [35, 36], (ii) by releasing various soluble damaging factors into the intercellular medium such as reactive oxygen species (ROS) [37], nitric oxide (NO) [38, 39] and cyto-c [40], which can penetrate into the nearby cells rapidly and cause DSBs and other base damages. Interestingly, p53 causes the release of BE signalling molecules such as cyto-c and ROS/NO; thus, further contributes to damaging signalling [39, 40]. Also, ATM, an upstream protein that phosphorylates p53 on DSBs, is important for the generation of damaging BE signalling [41]. For example, ATM depletion abrogates BE [42].

The concentration of ROS/NO molecules can rapidly increase in a soluble medium. There has been report that radiation-induced BE can be seen as fast as 5 min after irradiation. Thus, bystander signals are accepted as immediate as compared with the DSB repair that may take hours [43]. Owing to this rapid increase of intercellular carriers and bidirectional interaction between neighbour cells [44, 45], it is reasonable to approximate the bystander signal as a mean field of average concentration of damaging factors without considering intermediate steps. That is each interacting cell contributes to the global level of damaging factors in intercellular medium via releasing damaging factors in proportion to its x-level at that time.

To model the mean-field global coupling under DSBs, we introduce a coupling term to every single CFO in the population (5). The coupled system model of p53 network oscillators is shown in (5) and (6), where N is the number of cells in the population, the term $C(1/N)\sum_{k=1}^{N} x_k$ is an approximation to the mean field and the coupling coefficient C defines the strength of the excitatory diffusive coupling between oscillators via ATM variable. Thus, the model includes damage input from two sources: (i) internal damage r_i and (ii) bystander signal $C(1/N)\sum_{k=1}^{N} x_k$, which are known to be persistent [45]. With the non-zero coupling term C, theoretical conclusions of constraints (3) and (4) guaranteeing three-mode ability no more hold. Thus, we solely rely on numerical solutions to obtain information about an oscillator's mode.

$$\dot{x}_i = \frac{1}{\tau_{i,\,1}}\left(-x_i\left[r_i\left(x_i^2 - (a_i + b_i)x_i\right) + a_i b_i + c_i y_i - r_i d_i\right]\right) + C\frac{1}{N}\sum_{k=1}^{N} x_k \tag{5}$$

$$\dot{y}_i = \frac{1}{\tau_{i,\,2}}(z_i + m_i x_i - n_i y_i) \tag{6}$$

Assuming the heterogeneity among cells, the parameters of cells in a population are constructed by randomly perturbing the fixed parameters of the reference cell via updating formula ($\text{parameter}_{\text{new}} = (1 - \epsilon) * \text{parameter}_{\text{ref}} + \epsilon\,\xi$), where ξ is a random number drawn from a uniform distribution on the open interval (0, 1) and by selecting those parameters, which obey constraint inequalities (3) and (4), so that the individual CFOs have the three-mode ability. The value of ϵ and the number of CFOs N are chosen large enough to serve our intention of collecting sufficient and rich data for statistical analysis, which are 0.1 and 100, respectively.

Throughout the analyses, we choose the tunable mode design parameters (r_i and m_i) and coupling strength parameter (C) as independent variables; thus, we numerically solve the population under several different values of those independent variables. Then, we observe the statistical characteristics of oscillations – such as changes in phase, mean and variance of period – and interpret those characteristics from the perspective of cell fate decision. The global coupling parameter C is usually not conceivable in terms of one corresponding physical element; thus, it is not accessible directly for a measurement, and rather it is a synthetic parameter that refers to a coarse-grained model of a complex interaction resulting in a coupling mechanism behaviour. Thus, though the parameter C, which comes from the physical property of the intercellular medium, may not be a tunable parameter, in reality, to explore the possible dynamical properties of coupling in its fuller form, a range of coupling strength values are investigated.

3 Results

3.1 Coupling increases sensitivity to damage

Assuming that DNA damage severity is uniform across the population, i.e. $r_i = r_{\text{fixed}}$ for all i, (5) and (6) are solved for different r_{fixed} and C values. Since the population is heterogeneous, the sensitivity of cells toward the damage severity differs. At low r_{fixed} values, the percentage of cells oscillating, i.e. the percentage of cells responding to damage, is low (Fig. 2*a*). On the other hand, as r_{fixed} goes toward 1, the number of responding cells monotonically increases independently from the parameter C, and saturates at the population number. This is consistent with experimental data, which shows that the number of cells oscillating increases with the damage [46]. Also, the parameter C has monotonically increasing effect on the number of responding cells (Fig. 2*a*). Thus, the sensitivity of cells toward damage has increased with the introduction of coupling.

3.2 Damage severity r has monotonic decreasing effect on the mean and the variance of periods

Assuming $r_i = \text{r}_{\text{fixed}} = 1$ for all i and that cells do not interact ($C = 0$), the natural periods of the CFOs (i.e. the periods of independent CFOs) are found to range from 4.8 to 9.3 h with mean of 6.1 and the standard deviation of 0.83 h. In this case, the rate of oscillating cells is 100%, where 56% of the population exhibits 3–4 pulses of x_i-level in a 24 h period, whilst whole population range from 2.5 to 5.87 pulses. Compare this situation with $r_i = 0.7$ and $C = 0$, where only 9% of the population oscillates (Fig. 2*a*), at periods with a mean of 53 and standard deviation of 26 h (Fig. 2*b*). It is observed that as r_i goes to lower values, the rate of oscillating cells decreases, and the mean period of those oscillating cells has increased mean and increased standard deviation of oscillation period under $C = 0$ (Fig. 2*b*). This effect of r_{fixed} is also valid under non-zero C (Fig. 2*c*). The effect of damage severity on period characteristics is consistent with experimental data, which reveals that the distribution of periods become narrower and fraction of oscillating cells increases as the damage increases [46]. Thus, it can be said that the constructed population of cells with cell fate selection model defined by the sets of (1)–(4) successfully features the key properties of p53 dynamics.

© The Institution of Engineering and Technology 2019

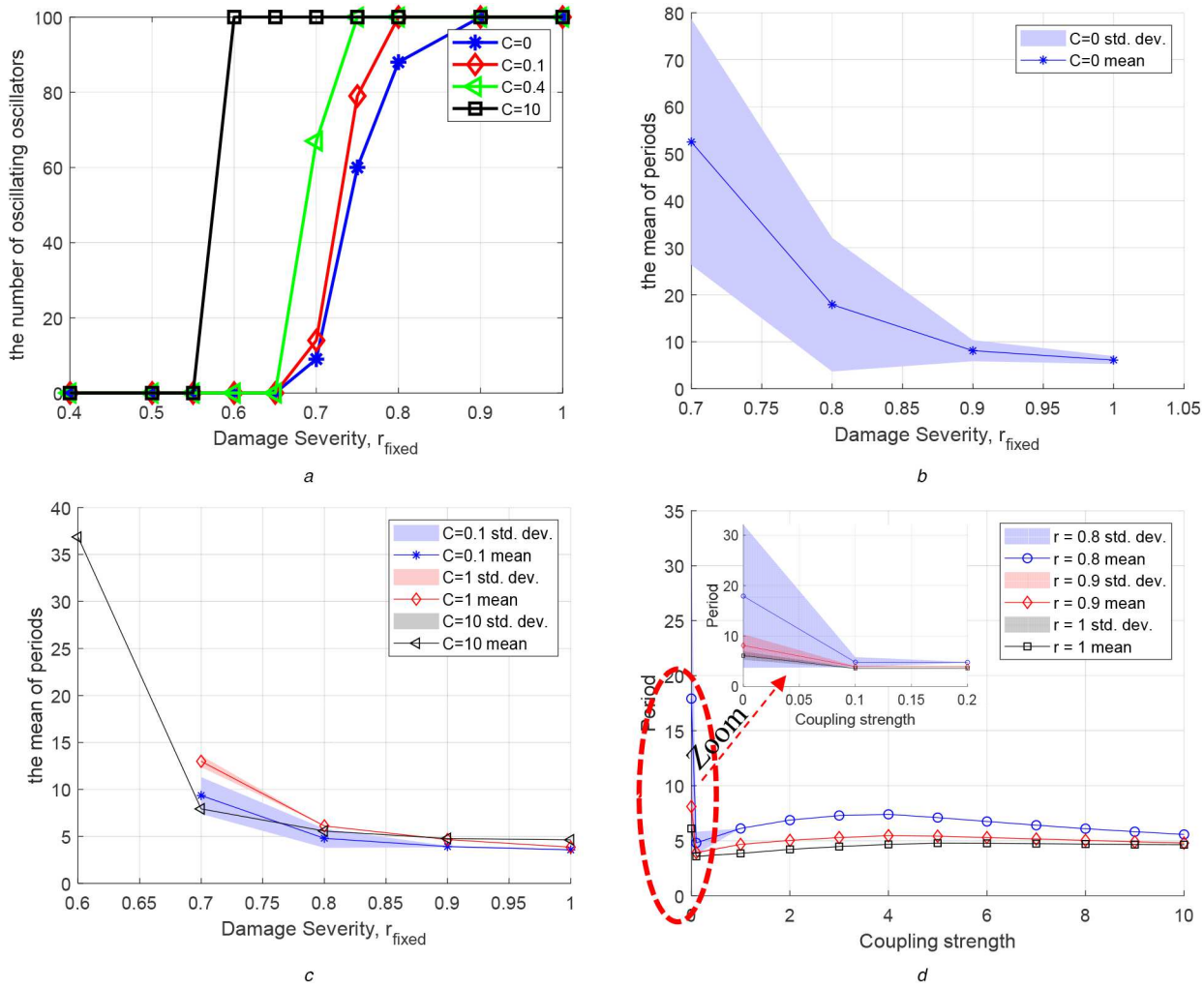


Fig. 2 *Statistical characteristics of oscillatory DNA damage response in the population under varying r_{fixed} and C values*

(a) Number of oscillating cells is zero until some threshold $r_{\text{fixed}} = r_{\text{threshold}}$. This threshold can be made smaller with increased C value. Additionally, C has increasing effect on the number of oscillatory response if r_{fixed} is greater than some thresholds. Independently from C, as the damage increases further, the number of oscillating cells increases after some threshold and saturates at the population number, 100, ***(b)*** Standard deviation of oscillating CFOs decreases as r_{fixed} increases, meaning that more uniform periods in the population are obtained as damage increases under $C = 0$, ***(c)*** Independently from C, damage has decreasing effect on the variations among periods as demonstrated for $C =$ 0.1 and 1, ***(d)*** Parameter C has vanishing effect on the standard deviation of periods. It also has non-monotonic decreasing effect on the mean of periods. The fast descend of trajectories after $C = 0$ is due to the introduction of coupling

3.3 Coupling parameter C has decreasing effect on the mean and the variance of periods

Assuming uniform damages across the population, i.e. $r_i = r_{\text{fixed}}$, we numerically solve the ensemble of oscillators for different r_{fixed} and C pairs: r_{fixed} being 0.8, 0.9 or 1 and C values ranging from 0 to 10. Then, we plot the mean of the periods as a line and standard deviations as a bound on the respective line in Fig. 2*d*. We observe that as the coupling strength among the oscillators increases, the mean oscillation period of the ensemble first decreases sharply and then after reaching a local minimum (at $C \cong 0.1$) it increases up to a local maximum point and then stabilises at a mean value as C goes higher (Fig. 2*d*). Nevertheless, the periods attained at the local maximum point is smaller than the periods attained in case of no coupling, i.e. $C = 0$. Thus, coupling strength has a non-monotonic decreasing effect on the mean oscillation periods. Another important effect of the term C is that it has monotonically decreasing effect on the variability of periods. As C is increased further, the variance of period tends to approach to zero (Fig. 2*d*), which is also indicative of a phase synchronisation among oscillators as will be investigated in Section 3.5.

3.4 Interpretation of further damaging on bystander cells by irradiated cells

For the proper functioning of cell fate mechanisms, there must be an optimal range of periods such that the repair must be finished before a circadian period (i.e. about 24 h) for repairable damages or apoptosis decision must be given for unrepairable damages. Any deviation from such optimal frequency range may pose several risks. Since the higher r_{fixed} values result in higher frequencies with lower variance in comparison with the case of lower r_{fixed}, one strategy to keep oscillations in a plausible range seems to be increasing the r_{fixed} value of the population, which can be achieved by a coupling mechanism that allows further damaging among cells in the population (Note that in reality, damage severities in a group differ from cell to cell; however, we assume a mean damage severity r_{fixed} which is the same for every cell.). Additionally, the coupling also causes further decreasing effect on the mean and variance of periods (Figs. 2*b–d*). This decreasing effect can be interpreted from two aspects: (i) the increased frequency of oscillations increases the average production of p53 over a fixed time interval; thus, maintaining more repair potentiality. This decreases the likelihood of a prolonged repair process for repairable damages, (ii) since pro-apoptotic factors accumulate over pulses of p53, they now accumulate faster favouring the apoptosis over cell survival as the severity of damage (r_{fixed}) increases. This forces cells to take the apoptosis decision faster for

© The Institution of Engineering and Technology 2019

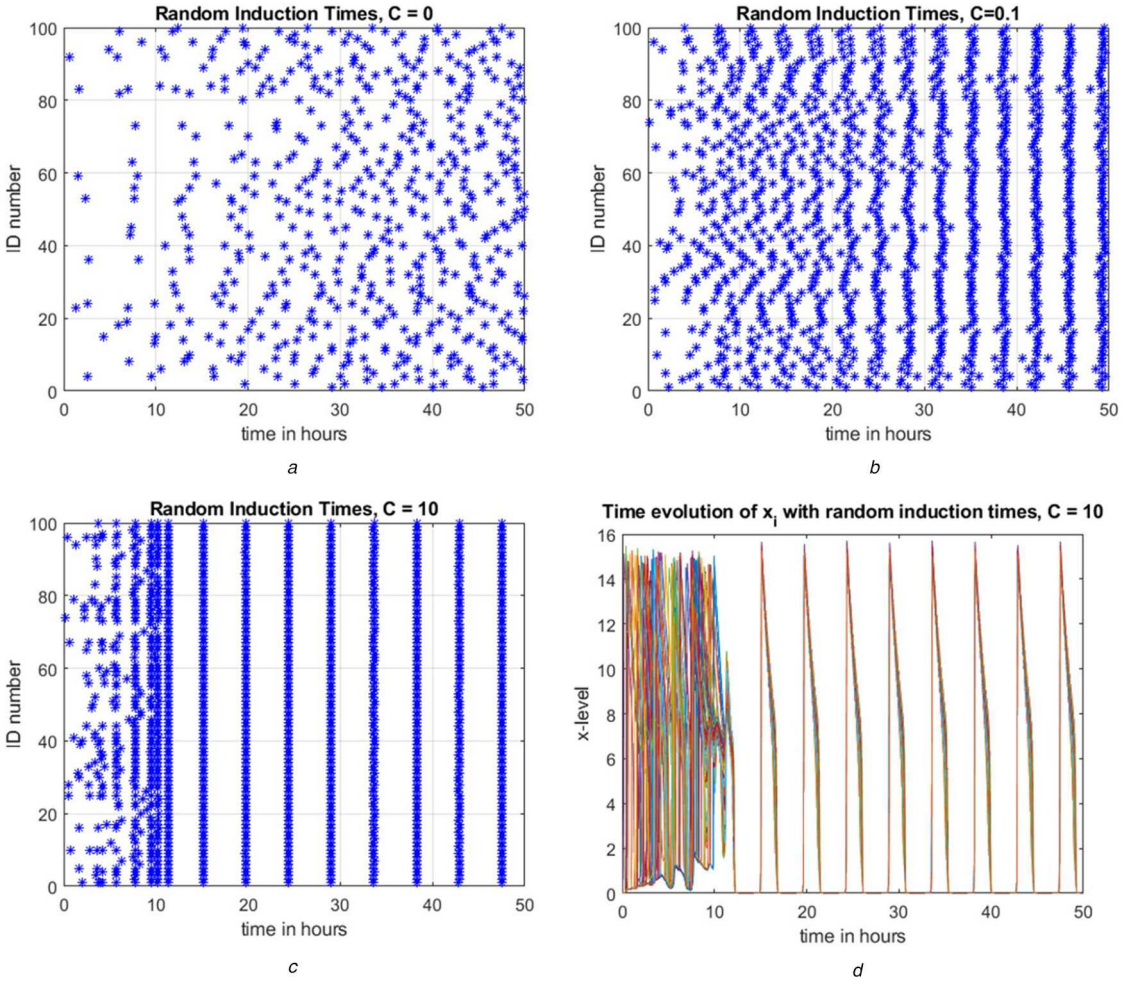


Fig. 3 *Phase synchronisation property when* $r_i = 1$ *for different coupling strength values under random induction times. The peaks of pulses when* ***(a)*** $C = 0$, ***(b)*** $C = 0.1$, ***(c)*** $C = 10$, ***(d)*** Time solution x_i levels of the population with random induction times for $C = 10$

unrepairable damages since more pulses can be produced in a less time. Furthermore, another important effect of increased r_{fixed} is that it increases the likelihood of a cell to oscillate, i.e. to respond to damage (Fig. 2*a*). Thus, we support the idea that high damaged cells have lower risk than low damaged cells, since a high damaged cell may repair the damage or choose to go to apoptosis via triggering an oscillatory response, whereas low damaged cells are not forced to take cell fate decision due to the failure of triggering oscillatory p53 response.

With an increase in r_{fixed}, cells in the group will have high repair potentiality decreasing the chances of unrepaired damage or go to apoptosis removing the risk of cancer. Thus, cells might be evolved to use coupling that is achieved by bystander damaging mechanism to improve the functionality of oscillations by adjusting their frequencies under difficult situations. Our hypothesis agrees with the observation of Type-1 BE, where the irradiated cells cause further damages in the unirradiated bystander cells and decrease the survival rates in bystander cells since they are forced to take cell fate decision. Also, it can be interpreted as an alert or warning mechanism for bystander cells [47].

3.5 Phase properties

Another important effect of the term C is that it has monotonically decreasing effect on the variability among periods. As C increases, the variance vanishes making oscillations firing at the same rhythms. Differently than the parameter r_i, the effect of coupling strength on frequencies has more complex dynamics on the overall population such as phase and frequency locking. We repeat the experiments for the cases of the damage received at the same or random times at each cell to investigate the characteristic of phase distribution. Since the time the damage is received determines the phase of the oscillation in uncoupled condition, we seek to understand the phase change in coupled condition regarding the uncoupled condition, and look for the advantages brought on from cell fate decision perspective.

We numerically solve the population of CFOs for the mode design parameters, $r_i = 1$ and $m_i = m_{i,\,\text{normal}}$ under $C \in [0, 10]$ with random damage induction times. Note that C is not increased indefinitely, since excessive C causes the oscillations to stop. Thus, we aim to cover a range of C values that make our point.

When $C = 0$ and $r_i = 1$, the phase pattern among cells seems to disperse as time goes by, as can be seen from Fig. 3*a* damages are induced randomly between 0 and 10 h. With the introduction of small coupling strength value, i.e. $C = 0.1$, there seems to be a stable phase pattern among cells (Fig. 3*b*). As the coupling strength increases, the phase difference among the oscillators tends to go zero. Observe that cells with DSBs induced at random times are synchronised at higher C values, e.g. $C = 10$ (Figs. 3*c*, *d*), and zero-phase difference seems to be a stable behaviour, whilst under certain small C, a dispersed phase pattern seems to be a stable behaviour.

Another critical observation is that with the introduction of the coupling, the responses to DSBs are obtained faster, as compared with the uncoupled case (Fig. 4). Since the pulses indicate the peak activity, we use the timing of the peak of the first pulse as the indicator of the response time toward DNA damage. Taking $r = 1$, the mean response time when the peaks of the first pulses of cells occur at the 0.35 h for $C = 0$, whilst the response time decreases toward 0.2 h as C goes to 10, which indicates an advantage of coupling in terms of response time (Fig. 4*b*). As the severity decreases, the response time toward DNA damage decreases, which indicates that more severe damages are responded more rapidly by the cell (Fig. 4*b*). Thus, the parameter r has a decreasing effect on the response time.

© The Institution of Engineering and Technology 2019

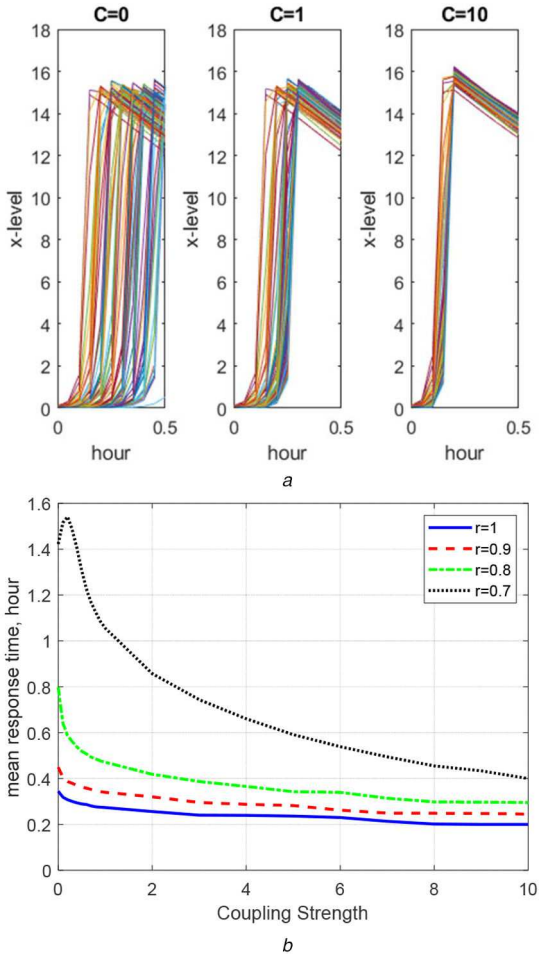


Fig. 4 *Mean response time of cells under different coupling strength values*

(a) First pulses of x_i levels on DNA damage induced at 0.1 h, ***(b)*** Averaged time of peaks of first pulses on DNA damage induced at 0.1 h with different damage severities

What might be the possible biological advantages of zero-phase pattern or dispersed phase pattern behaviours? Our results indicate that even with the introduction of a small coupling value, which does not lead to zero-phase synchronisation, e.g. $C = 0.1$ (Fig. 3*b*), the benefits such as decreased mean response time, decreased variance of periods, decreased mean of periods and increase in the number of responsive cells are still observed (Fig. 2), though higher C values leading to a zero-phase synchronisation deliver those benefits to the higher degrees, e.g. $C = 10$ (Fig. 2). This case is different from other biological oscillators, where the zero-phase synchronisation is critical such as in heart pulsing and suprachiasmatic nucleus generating circadian rhythm. Phase synchronisation in p53 network may be a by-product of an evolutional intention to keep rhythms in an optimal range. Thus, we claim that zero-phase synchronisation may not be observed in wet-lab experiments of BE; however, the benefits of the coupling can be observed.

To validate such behaviour in wet lab, one can record isolated single-cell oscillations and compare them with the oscillations of the cells sharing the same medium. Additionally, one can search for the existence of zero-phase synchronisation when C is set to higher values via manipulating BE communication mechanisms in wet lab such as by further activating ROS/NO producing gene regulatory networks. We believe that the scarcity of *in-silico* studies of BE is due to its study at the phenomenological (tissue) level such as increase and decrease in cell survivals. Our analyses may give directions for experimentalists to study BE in systems level, e.g. to study ROS/NO as a target to manipulate cell fate decisions. Such wet-lab studies may boost *in-silico* studies of BE phenomenon.

3.6 Coupling in p53 network may underlie BE types

In this section, we aim to deliver numerical evidence (a heuristic argument) that coupling in p53 network may underlie Type-2 and Type-3 behaviours. For this, we mimic the wet-lab experiments *in-silico*. We construct two groups of cells: one with low severity of damage (Group-1) and one with high severity of damage (Group-2), which is assumed to be caused by low and high-irradiated doses as in wet-lab experiments [2]. We investigate the cell fate decision tendencies in those groups in four cases: (i) Group-1 isolated (with no interaction of Group-2), (ii) Group-2 isolated, (iii) Group-1 interacting with Group-2 and (iv) Group-2 interacting with Group-1. Since the interaction is bidirectional, in fact cases III and IV are carried out in a single experimental setup. We aim to demonstrate the increase in cell survivals in cases (iii) and (iv) in comparison with the cases (i) and (ii), respectively, by numerically investigating the effect of coupling strength C on the mode design parameters' (r_i and m_i) choice of cell fate decisions. However, since the exact values of cell fate determinants (r_i, m_i values of cells and C value) are not known, we carry out simulations of these four cases under several values of these parameters and seek to find at least one parametric combination or a region that can demonstrate Type-2 and Type-3 behaviours. If we can find such a parametric region, then it can be hypothesised that coupling in p53 network is a candidate mechanism that underlies Type-2 and Type-3 behaviours observed in wet-lab experiments. Such claim would be invaluable to encourage further studies for constructing more detailed and complex models to investigate BEs *in-silico* as well as *in vitro* or *in vivo*, and understand the incomprehensible parts of BE phenomenon.

Experimental setup: The previously constructed 100 cells of population is split into two groups: the cells with ID numbers $1-50$ into Group-1 and the cells with ID numbers 51–100 into Group-2. Here, r_i parameters of Group-1 are set to $r_i = r_{\text{low}}$, whilst r_i parameters of Group-2 is set to $r_i = r_{\text{high}}$, where $0 < r_{\text{low}} < r_{\text{high}} \leq 1$ assuming uniform damage severity inside the groups. In this section, we only show the results for $r_{\text{low}} = 0.6$ and $r_{\text{high}} = 1$, which has a parametric region of C and m_i combinations that seem to replicate Type-2 and Type-3 behaviours. After fixing the r_i parameters of the groups, there remain two independent variables C and m_i. Note that m_i, which differs from cell to cell, is gradually decreased to drive the ith cell to high x_i-level, i.e. apoptosis, as a consequence of two-phase dynamics property. Thus, rather than its exact value, its relative value to normal value is important for cell fate decision. Thus, to model the relative change, we introduce $m_{i,\text{new}} = m_{i,\text{old}} \times m_k$, where $m_k \in [0,\ 1]$ and m_k is assumed same for every cell in the population. By doing this, we can gain a quantitative insight into the tendency of the whole group to apoptosis by changing one parameter, i.e. m_k. Another advantage of such transformation is that m_k, but not m_i, can be used as an axis of a coordinate plane for the whole group investigation.

We construct heatmaps using C and m_k parameters, where $C \in [1,\ 10]$ and $m_k \in [0,\ 1]$ as the axes of the heatmap, which illustrate the cell fate decisions in a group for the corresponding $C - m_k$ combinations in Figs. 5 and 6: the number of oscillating cells in first row and the number of cells with high x_i-level in the second row for the corresponding $C - m_k$ combination under the four cases above. The remaining number of cells indicate cells with low x_i levels and are not shown in any figure due to length constraints.

In Figs. 5*a* and *b*, $C - m_k$ graphs for cell fate decisions in isolated Group-1, i.e. case (i), whilst in Figs. 5*d–f* Group-1 interacting with Group-2, i.e. case (iii) is depicted. In case (i), oscillations are observed for $C = 10$ and $m_k \in [0.4 - 1]$ (Fig. 5*a*). Apoptosis is observed for $C \in [9,\ 10]$ and $m_k \in [0.1 - 0.3]$ (Fig. 5*b*). In other $C - m_k$ combinations, CCP is observed. Thus, we conclude that Group-1 has oscillatory behaviour only for a small range of $C - m_k$ combinations and irresponsive to damage for most $C - m_k$ combinations. This graph indicates the possibility of

© The Institution of Engineering and Technology 2019

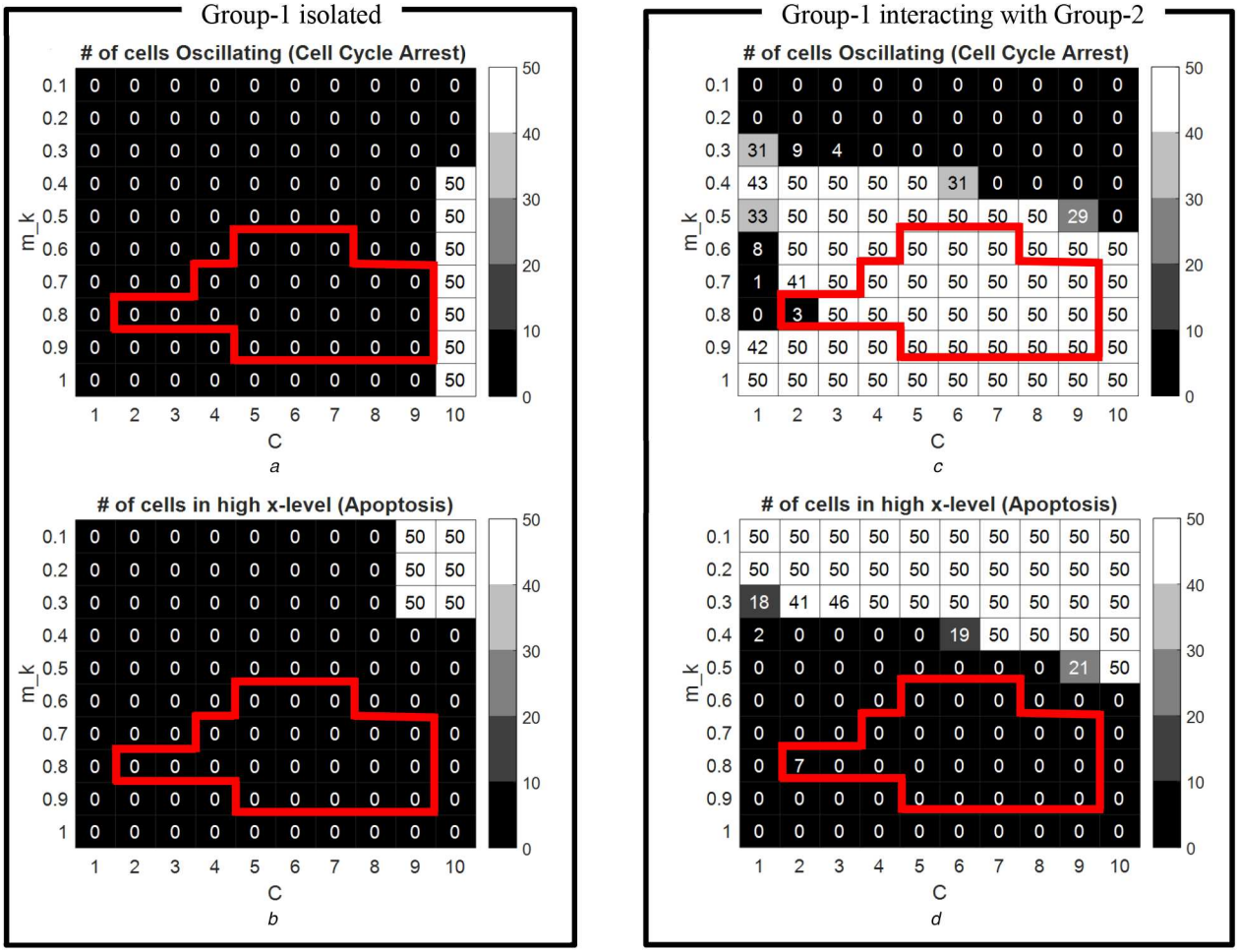


Fig. 5 *$C - m_k$ heatmaps of Group-1 in*
*(**a, b**)* Isolated, *(**c, d**)* Interacting cases

inactivation of p53 network in those cells, which results in low repair activity increasing the possibility of leaving the damage unrepaired, which is consistent with the experimental observation that low-dose applied cells do not trigger repair function [48]. It is known that persistent DNA damage can make cell go to apoptosis through other pathways such as NF-KB, which is known to be involved in BE [32]. Thus, we assume that cell death in Group-1 with inactivated p53 network results from involving other pathways due to ineffective repairing.

In Figs. 6*a* and *b*, $C - m_k$ graphs for cell fate decisions in isolated Group-2 are seen. It can be seen that Group-2 has oscillatory response for all $C \in [1, 10]$ and $m_k = 1$. Also, it can be seen that Group-2 either goes to apoptosis or oscillates, but no CCP for any $C - m_k$ combination, meaning that Group-2 is more responsive to damage than Group-1. Additionally, in comparison with Group-1, Group-2 has more tendency to go to apoptosis since a slight decrease from normal $m_{i,\,\text{normal}}$ value may cause apoptosis in Group-2 (e.g. 0.10% decrease in m_i caused by $m_k = 0.9$ when $C > 5$). Thus, we assume that cell death in Group-2 results from activation of oscillatory p53 network, which causes a decrease in m_i parameter in every pulse, and eventually drive the cell to apoptosis.

When the two groups are allowed to interact, the resulting $C - m_k$ heatmaps are depicted in Figs. 5*d, e* and 6*c, d*. In this case, we are looking for any $C - m_k$. Combination that results in a higher repair potentiality such as changing dynamics from low level to oscillations or apoptosis to oscillations, since it is suggested that enhancement in cell survivals in Type-2 and Type-3 may be due to enhanced repair activity [2]. From another perspective, $C - m_k$ heatmaps can be interpreted as analysis under parameter uncertainties instead of looking for a $C - m_k$ pair that replicates Type-2 and Type-3 behaviours. Thus, when comparing Fig. 5*a* with Fig. 5*d*, it can be seen that Group-1 has more oscillatory region in $C - m_k$ graph when interacting with Group-2 under parametric uncertainties. Additionally, Group-1 interacting with Group-2 is more responsive under parametric uncertainties in comparison with the case of isolated Group-1, since CCP region shrinks in the interacting case (Figs. 5*e* and *f*). Type-2 behaviour is said to exist in certain $C - m_k$ pairs, where the number in a grid cell in Fig. 5*d* is greater than the same grid cell in Fig. 5*a*. The $C - m_k$ pairs in the marked region in Fig. 5 are examples of Type-2 behaviour (note that the marked region indicates, where Type-2 and Type-3 behaviours are observed at the same time as will be discussed in the next paragraphs, thus the marked region is smaller than the actual region where Type-2 is observed).

Also when comparing Fig. 6*a* with Fig. 6*d*, Group-2 has more oscillatory region under parametric uncertainties when interacting with Group-1, i.e. case (iv), in comparison with the isolated case, i.e. case (ii). Thus, when considering Figs. 5 and 6, oscillatory region is expanded in both groups. A region with red borderline indicates the coexistence of increase in cell survivals in both groups, i.e. the coexistences of Type-2 and Type-3 behaviours in a single experiment.

For instance, choosing $C = 5$, it can be seen that isolated Group-1 does not have oscillatory region for any m_k value (Fig. 5*a*), whilst in the interacting case, Group-1 has an oscillatory region for $m_k \in [0.4,\ 1]$ (Fig. 5*d*). Thus, Group-1 has an expanded oscillatory region under parametric uncertainties in the interacting case, which is an indicator for the Type-2 behaviour. Next, we show that also Group-2 has expanded oscillatory region. In Fig. 6*a*, it can be seen that for $C = 5$ isolated Group-2 has oscillatory characteristics when $m_k \in [0.9, 1]$, whilst in the interacting case Group-2 has oscillatory characteristics when $m_k \in [0.6, 1]$. In other words, in interacting case of Group-2, apoptosis is seen if m_k is

© The Institution of Engineering and Technology 2019

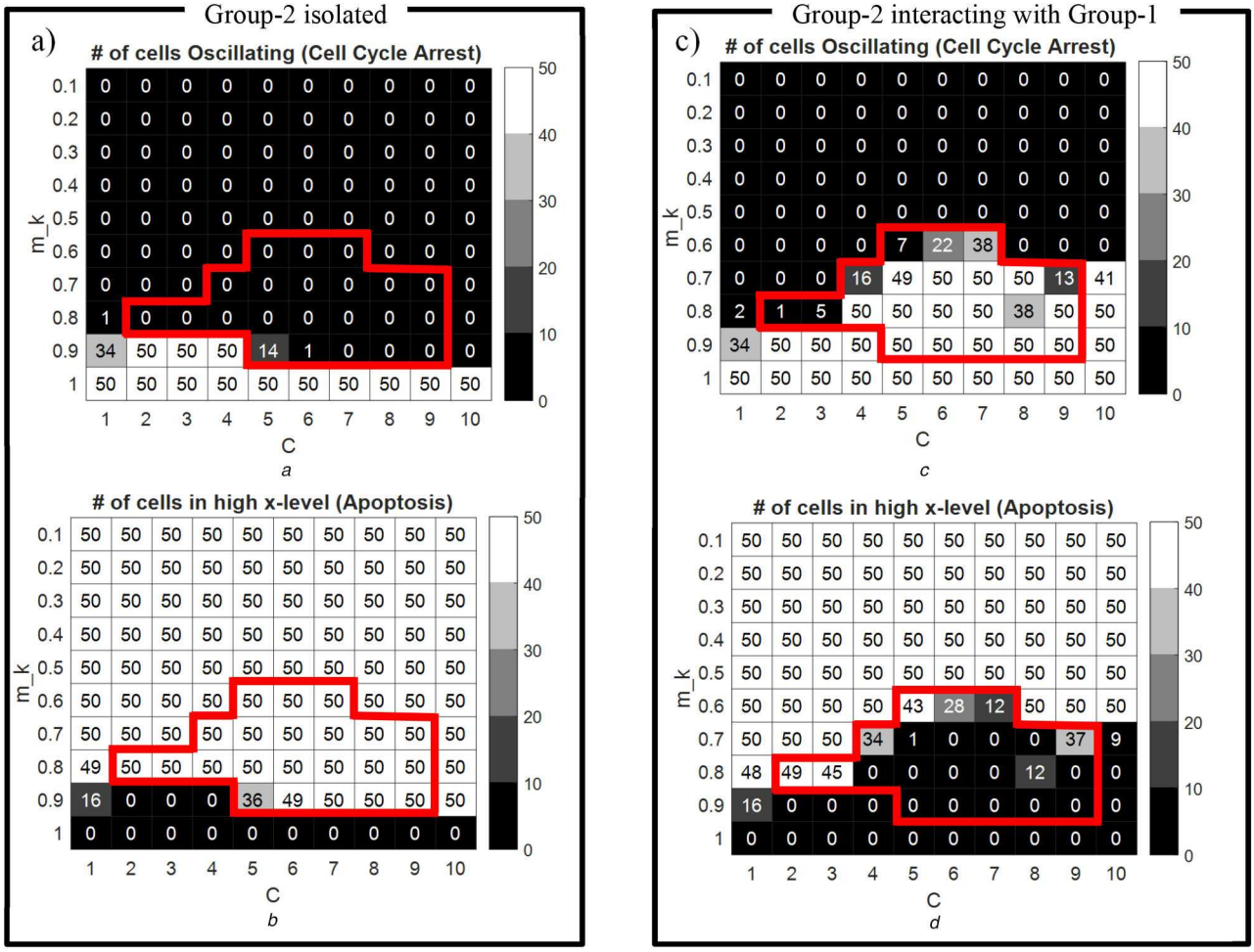


Fig. 6 *$C - m_k$ heatmaps of Group-2 in* ***(a, b)*** *Isolated,* ***(c, d)*** Interacting cases

dropped below 0.6, whilst in the case of isolated Group-2, apoptosis is seen if m_k is dropped below 0.9. Thus, in the interacting case, more pulse activity is needed to drive Group-2 to apoptosis since in every pulse m_k decreases according to the two-phase dynamics model of the p53 network. Thus, we conclude that oscillations (i.e. repair or cell survival) are favoured over sustained high x_i-level (i.e. apoptosis) in interacting Group-2. Such parametric combinations indicate Type-3 behaviour.

In Fig. 7, we demonstrate the increase in oscillatory region via time evolutions of x_i levels in both groups with one example of $C - m_k$ pair, i.e. $C = 8$ and $m_k = 0.8$. Note that in such combination, isolated Group-1 has low x_i-level (Fig. 7*a*). When interacting with Group-2, all cells in Group-1 starts to oscillate (Fig. 7*b*). Isolated Group-2 goes to sustained high x-level (Fig. 7*c*). When interacting with Group-1, some cells in Group-2 starts to oscillate, raising the likelihood of increased cell survival in Group-2. Thus, both Type-2 and Type-3 behaviours are observed in such $C - m_k$ pair.

4 Discussion

We further analyse the interaction between Group-1 and Group-2. In Fig. 8, the change in oscillation regions in Group-1 and Group-2 are depicted for the following damage severities: (i) $r_i = 0.7$ for $i \in \{1, 2, \ldots, 50\}$ and $r_i = 1$ for $i \in \{51, 52, \ldots, 100\}$, (ii) $r_i = 0.8$ for $i \in \{1, 2, \ldots, 50\}$ and $r_i = 1$ for $i \in \{51, 52, \ldots, 100\}$ and (iii) $r_i = 0.9$ for $i \in \{1, 2, \ldots, 50\}$ and $r_i = 1$ for $i \in \{51, 52, \ldots, 100\}$. We have observed that the oscillatory region of Group-1 interacting with Group-2 shrinks as the severity of Group-1 increases (Fig. 8*a*) and also an oscillatory region of Group-2 shrinks as the severity of Group-1 increases (Fig. 8*b*). Giving the fact that intra and intercellular mediums are a highly noisy environment, a larger oscillatory region would increase the likelihood of observing the Type-2 and Type-3 behaviours. Thus, for better analysis in the wet lab, one group must be given sufficiently low irradiation, which is in agreement with the literature view.

We interpret the rescue effect, which is described as increase in cell survival in high-irradiated group interacting with no-dose applied group in the context of Type-3 behaviour. Since Type-3 behaviour can be observed in case of interaction with sufficiently low-irradiated group, no-dose applied group can reach to that level of sufficiency by receiving further damaging from high-irradiated group. Thus, we hypothesise that the rescue effect behaviour can be categorised as Type-3 behaviour. However, this reasoning needs further validations by experimentalists.

BE has been considered to be used in radiotherapy; however, the methods have not been fully elucidated [10]. We suggest that the manipulation of coupled oscillatory p53 network might have potential usage in cancer therapy along with BE phenomenon, as a combination therapy. Since as C value increases, the likelihood of a cell going to apoptosis increases (Figs. 5*a* and 6*a*), when a group of cell is targeted for radiotherapy, the same effective killing may be obtained with lower doses, but increased C value. This would decrease the side effects of radiotherapy. For such approach, drugs that increase coupling term C may be used such as drugs that further activate ROS/NO cellular pathways.

Herein, we have carried out *in-silico* experiments to compare the cooperative response of cells mediated by coupling and the response of single cell in isolation. We showed that the cooperative response gives better DNA damage response. First, the number of oscillating cells, i.e. responding cells, increases with coupling. Second, the analysis on the distribution of periods on DSB induction showed that periods that are more effective are obtained in case of coupling and that cells give response more rapidly.

© The Institution of Engineering and Technology 2019

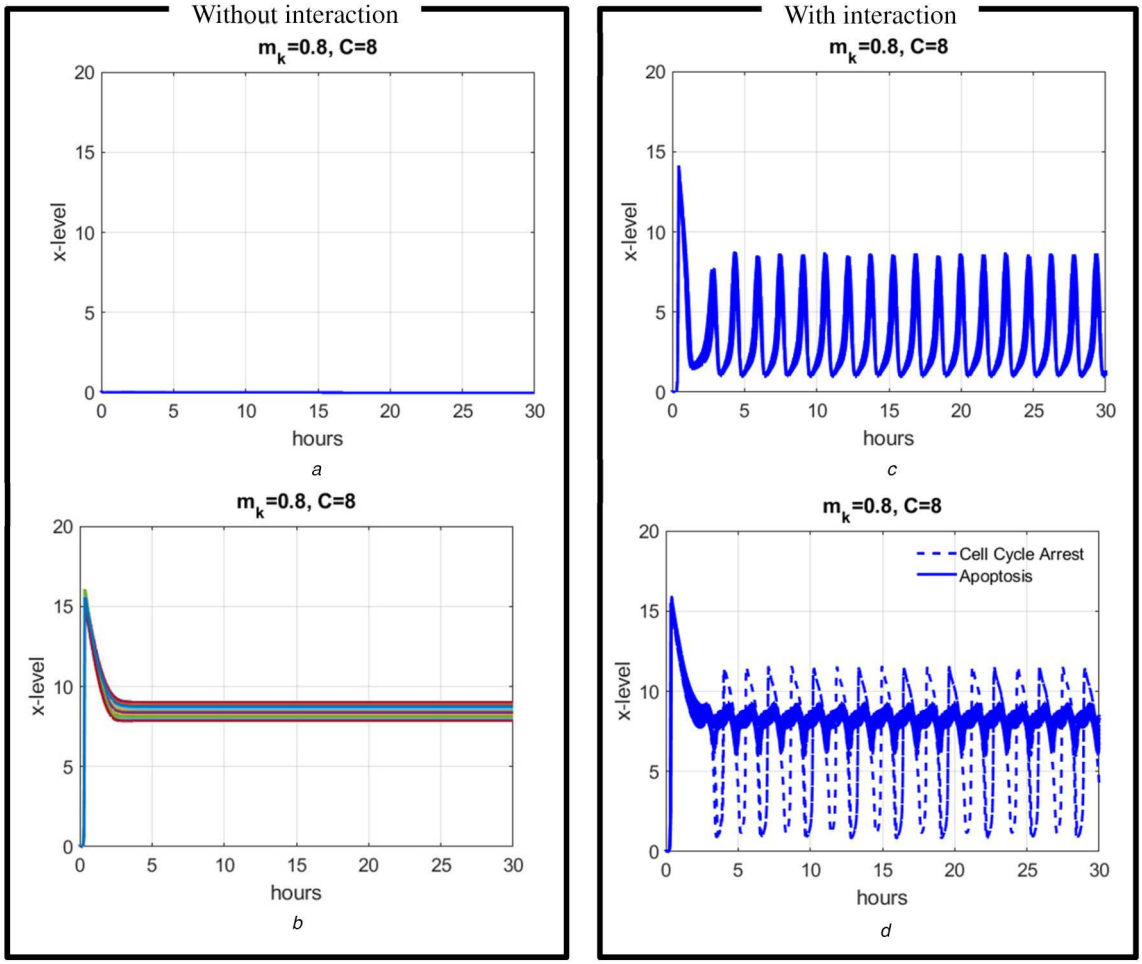


Fig. 7 *Demonstration of Type-2 and Type-3 behaviours for* $C = 8$ *and* $m_k = 0.8$

(a) Isolated Group-1 exhibits low x_i level, ***(b)*** Isolated Group-2 has sustained high x_i-level, ***(c)*** Interacting Group-1 oscillates, ***(d)*** Some cells in interacting Group-2 oscillates

Third, the coupling widens the parametric region that leads to oscillations, thus response.

Furthermore, these positive effects are obtained even if there is no zero-phase synchronisation. Thus, zero-phase synchronisation is not essential to benefit from coupling as in other biological oscillators. We conclude that single-cell response cannot be thoroughly understood without considering the effect of cooperative behaviour since the coupling is an important parameter that affects the characteristics of p53 oscillations in a single cell.

By carrying out further analysis of the proposed mathematical framework, we claim that types of BE are all the results of a dynamic property emerging from the same mechanism, i.e. coupling of p53 network oscillators. We believe that this provides an explanation and insight into BE behaviours in cells. The proposed framework can be used as a reference for modelling more detailed interactions in further studies. Further studies may also include the repair process, e.g. integrated microdosimetric-kinetic models [12], to create agent-based models that replicate experimental data.

Experimental studies can target the mode design parameters m_k, r and C to support our hypothesis that BEs are manifestations of dynamic property emerging from the coupling of the p53 network. Wip1 inhibitors [(Wip1 is the variable y_i in (2)] such as Wip1 selective antagonist GSK2830371 [49], can be used to manipulate m_k. Enhancers or inhibitors of ROS/NO production pathways such as proline oxidase, [50] or NQO1 [51], can be used to manipulate coupling strength parameter C. Then, one can construct $C - m_k$ heatmaps as in Figs. 5 and 6 or looking for such range of parameters that would replicate Fig. 7, to observe Type-2 and Type-3 behaviours in terms of p53 dynamics, which would validate our hypothesis.

After the validation of our hypothesis, $C - m_k$ heatmaps can be constructed for specific cell lines, so that the combination therapies using ROS/NO enzymes, Wip1 inhibitors and radiation therapy for specific tumours can be developed. Indeed, such approaches are already being tested by experimentalists [49–52]. Moreover, our model can help to understand such approaches.

5 Conclusion

Herein, we have proposed a coupled framework based on three-mode p53 network oscillator to study BE phenomenon. On the basis of that framework, the effect of coupling on the transition between the modes is studied. Our analyses emphasise that the coupling of p53 network oscillators is a candidate that underlies BE phenomenon especially when considering the fact that enhanced repair mechanisms might involve. Oscillatory characteristics of p53 dynamics in single cells that are affected by the coupling mechanism is a potential subject, which may be used to increase the effectiveness of radiotherapy. Future studies may use parametric analysis to investigate the cell fate decisions under noise. Additionally, instead of manipulating parameters externally, higher-dimensional cell fate models that manipulate those parameters internally can be developed to replicate wet-lab environment *in-silico*.

© The Institution of Engineering and Technology 2019

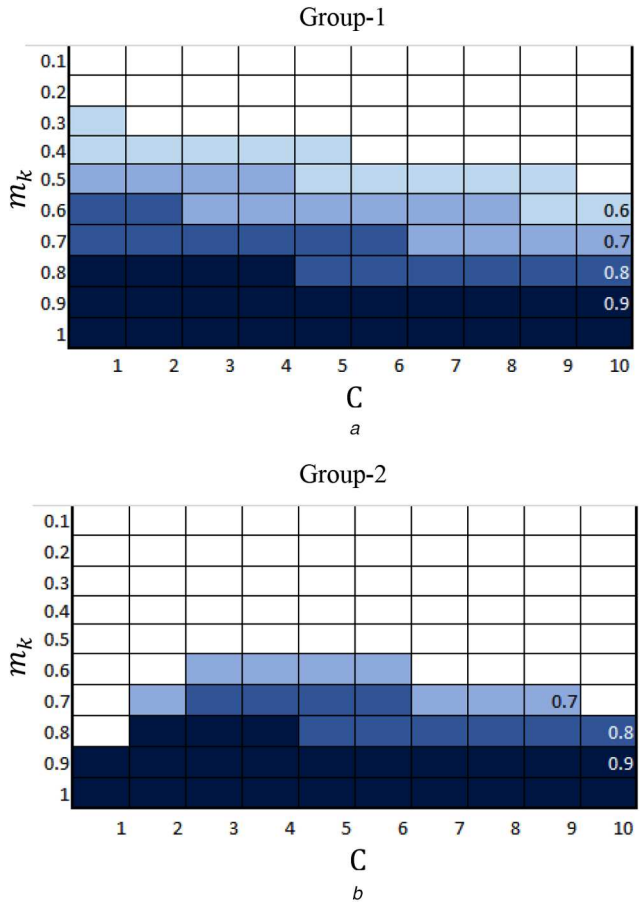


Fig. 8 *Change in oscillation regions in Group-1 and Group-2*
(a) Oscillatory regions of Group-1 interacting with Group-2 with $r_i = 1$, as the damage severity of Group-1 increases from 0.6 to 0.9. As the damage severity of Group-1 changes from 0.6 to 0.9, the oscillatory region shrinks, ***(b)*** Oscillatory regions of Group-2 with $r_i = 1$, interacting with Group-1 as the damage severity of Group-1 increases from 0.7 to 0.9. As the damage severity of Group-1 changes from 0.7 to 0.9, the oscillatory region of Group-2 shrinks. Note that, other regions hide oscillatory region for 0.6 (see Fig. 6*b*)

6 References

[1] Mothersill, C., Rusin, A., Fernandez-Palomo, C., *et al.*: 'History of bystander effects research 1905-present; what is in a name?', *Int. J. Radiat. Biol.*, 2018, **94**, (8), pp. 696–707

[2] Mackonis, E., Suchowerska, N., Zhang, M., *et al.*: 'Cellular response to modulated radiation fields', *Phys. Med. Biol.*, 2007, **52**, (18), pp. 5469–5482

[3] Chen, S., Zhao, Y., Han, W., *et al.*: 'Rescue effects in radiobiology: unirradiated bystander cells assist irradiated cells through intercellular signal feedback', *Mutat. Res./Fundam. Mol. Mech. Mutagen.*, 2011, **706**, (1), pp. 59–64

[4] Marín, A., Martín, M., Liñán, O., *et al.*: 'Bystander effects and radiotherapy', *Rep. Pract. Oncol. Radiother.*, 2015, **20**, (1), pp. 12–21

[5] Fernandez-Palomo, C., Seymour, C., Mothersill, C.: 'Inter-relationship between low-dose hyper-radiosensitivity and radiation-induced bystander effects in the human T98G glioma and the epithelial HaCaT cell line', *Radiat. Res.*, 2016, **185**, (2), pp. 124–133

[6] Yang, G., Li, W., Jiang, H., *et al.*: 'Low-dose radiation may be a novel approach to enhance the effectiveness of cancer therapeutics', *Int. J. Cancer*, 2016, **139**, (10), pp. 2157–2168

[7] Schoenherr, D., Krueger, S., Martin, L., *et al.*: 'Determining if low dose hyper-radiosensitivity (HRS) can be exploited to provide a therapeutic advantage: a cell line study in four glioblastoma multiforme (GBM) cell lines', *Int. J. Radiat. Biol.*, 2013, **89**, (12), pp. 1009–1016

[8] Peng, V., Suchowerska, N., Esteves, A., *et al.*: 'Models for the bystander effect in gradient radiation fields: range and signalling type', *J. Theor. Biol.*, 2018, **455**, (1), pp. 16–25

[9] Powathil, G.G., Adamson, D.J.A., Chaplain, M.A.J.: 'Towards predicting the response of a solid tumour to chemotherapy and radiotherapy treatments: clinical insights from a computational model', *PLoS Comput. Biol.*, 2013, **9**, (7), p. e1003120

[10] Powathil, G.G., Munro, A.J., Chaplain, M.A., *et al.*: 'Bystander effects and their implications for clinical radiation therapy: insights from multiscale in silico experiments', *J. Theor. Biol.*, 2016, **401**, (1), pp. 1–14

[11] Hattori, Y., Yokoya, A., Watanabe, R.: 'Cellular automaton-based model for radiation-induced bystander effects', *BMC Syst. Biol.*, 2015, **9**, (1), pp. 90–112

[12] Matsuya, Y., Sasaki, K., Yoshii, Y., *et al.*: 'Integrated modelling of cell responses after irradiation for DNA-targeted effects and non-targeted effects', *Sci. Rep.*, 2018, **8**, (1), pp. 4849–4863

[13] Kashino, G., Prise, K., Schettino, G., *et al.*: 'Evidence for induction of DNA double-strand breaks in the bystander response to targeted soft X-rays in CHO cells', *Mutat. Res./Fundam. Mol. Mech. Mutagen.*, 2004, **556**, (1), pp. 209–215

[14] Sokolov, M., Smilenov, L., Hall, E., *et al.*: 'Ionizing radiation induces DNA double-strand breaks in bystander primary human fibroblasts', *Oncogene*, 2005, **24**, (49), pp. 7257–7265

[15] Nagasawa, H., Huo, L., Little, J.: 'Increased bystander mutagenic effect in DNA double-strand break repair-deficient mammalian cells', *Int. J. Radiat. Biol.*, 2003, **79**, (1), pp. 35–41

[16] Sokolov, M., Dickey, J., Bonner, W., *et al.*: 'H2AX in bystander cells: not just a radiation-triggered event, a cellular response to stress mediated by intercellular communication', *Cell Cycle*, 2007, **6**, (18), pp. 2210–2212

[17] Purvis, J.E., Karhohs, K.W., Mock, C., *et al.*: 'P53 dynamics control cell fate', *Science*, 2012, **336**, (6087), pp. 1440–1444

[18] Purvis, J., Lahav, G.: 'Encoding and decoding cellular information through signaling dynamics', *Cell*, 2013, **152**, (5), pp. 945–956

[19] Koturbash, I., Loree, J., Kutanzi, K., *et al.*: '*In vivo* bystander effect: cranial X-irradiation leads to elevated DNA damage, altered cellular proliferation and apoptosis, and increased p53 levels in shielded spleen', *Int. J. Radiat. Oncol. Biol. Phys.*, 2008, **70**, (2), pp. 554–562

[20] Strigari, L., Mancuso, M., Ubertini, V., *et al.*: 'Abscopal effect of radiation therapy: interplay between radiation dose and p53 status', *Int. J. Radiat. Biol.*, 2014, **90**, (3), pp. 248–255

[21] Grosovsky, A.: 'Radiation-induced mutations in unirradiated DNA', *Proc. Natl. Acad. Sci.*, 1999, **96**, (10), pp. 5346–5347

[22] Kim, J., Jackson, T.: 'Mechanisms that enhance sustainability of p53 pulses', *PloS One*, 2013, **8**, (6), p. e65242

[23] Devi, G., Alam, M., Singh, R.: 'Synchronization in stress p53 network', *Math. Med. Biol.: J. IMA*, 2015, **32**, (4), pp. 437–456

[24] Liu, A.C., Welsh, D.K., Ko, C.H., *et al.*: 'Intercellular coupling confers robustness against mutations in the SCN circadian clock network', *Cell*, 2007, **129**, (3), pp. 605–616

[25] Kellogg, R.A., Tay, S.: 'Noise facilitates transcriptional control under dynamic inputs', *Cell*, 2015, **160**, (3), pp. 381–392

[26] Li, Q., Wang, Y.: 'Coupling and internal noise sustain synchronized oscillation in calcium system', *Biophys. Chem.*, 2007, **129**, (1), pp. 23–28

[27] Weiss, R., Knight, T.: 'Engineered communications for microbial robotics'. Int. Workshop on DNA-based Computers, Berlin, June 2000, pp. 1–16

[28] Gonze, D.: 'Modeling circadian clocks: from equations to oscillations', *Open Life Sci.*, 2011, **6**, (5), pp. 699–711

[29] Gonze, D.: 'Modeling circadian clocks: roles, advantages, and limitations', *Open Life Sci.*, 2011, **6**, (5), pp. 712–729

[30] Demirkıran, G., Demir, G.K., Güzeliş, C.: 'Two-dimensional polynomial type canonical relaxation oscillator model for p53 dynamics', *IET Syst. Biol.*, 2018, **12**, (4), pp. 138–147

[31] Batchelor, E., Mock, C.S., Bhan, I., *et al.*: 'Recurrent initiation: a mechanism for triggering p53 pulses in response to DNA damage', *Mol. Cell*, 2008, **30**, (3), pp. 277–289

[32] Lam, R., Fung, Y., Han, W., *et al.*: 'Rescue effects: irradiated cells helped by unirradiated bystander cells', *Int. J. Mol. Sci.*, 2015, **16**, (2), pp. 2591–2609

[33] Zhang, X.-P., Liu, F., Wang, W.: 'Two-phase dynamics of p53 in the DNA damage response', *Proc. Natl. Acad. Sci.*, 2011, **108**, (22), pp. 8990–8995

[34] Demirkıran, G., Demir, G.K., Güzeliş, C.: 'A canonical 3-D P53 network model that determines cell fate by counting pulses', *Electrica*, 2018, **18**, (2), pp. 284–291

[35] Peixoto, P., Ryu, S., Pruzansky, D., *et al.*: 'Mitochondrial apoptosis is amplified through gap junctions', *Biochem. Biophys. Res. Commun.*, 2009, **390**, (1), pp. 38–43

[36] Azzam, E.I., de Toledo, S.M., Little, J.B.: 'Direct evidence for the participation of gap junction-mediated intercellular communication in the transmission of damage signals from α-particle irradiated to non-irradiated cells', *Proc. Natl. Acad. Sci.*, 2001, **98**, (2), pp. 473–478

[37] Nowicki, M.O., Falinski, R., Koptyra, M., *et al.*: 'CR/ABL oncogenic kinase promotes unfaithful repair of the reactive oxygen species-dependent DNA double-strand breaks', *B. Blood*, 2004, **104**, (12), pp. 3746–3753

[38] Yakovlev, V.A.: 'Redox biology role of nitric oxide in the radiation-induced bystander effect', *Redox Biol.*, 2015, **6**, pp. 396–400

[39] Han, W., Wu, L., Chen, S., *et al.*: 'Constitutive nitric oxide acting as a possible intercellular signaling molecule in the initiation of radiation-induced DNA double-strand breaks in non-irradiated bystander cells', *Oncogene*, 2007, **26**, (16), pp. 2330–2339

[40] He, M., Zhao, M., Shen, B., *et al.*: 'Radiation-induced intercellular signaling mediated by cytochrome-c via a p53-dependent pathway in hepatoma cells', *Oncogene*, 2011, **30**, (16), pp. 1947–1955

[41] Hagelstrom, R., Askin, K., Williams, A., *et al.*: 'DNA-PKcs and ATM influence generation of ionizing radiation-induced bystander signals', *Oncogene*, 2008, **27**, (53), pp. 6761–6769

[42] Ghosh, S., Ghosh, A., Krishna, M.: 'Role of ATM in bystander signaling between human monocytes and lung adenocarcinoma cells', *Mutat. Res./ Genet. Toxicol. Environ. Mutagen.*, 2015, **794**, (1), pp. 39–45

[43] Hu, B., Wu, L., Han, W., *et al.*: 'The time and spatial effects of bystander response in mammalian cells induced by low dose radiation', *Carcinogenesis*, 2006, **27**, (2), pp. 245–251

[44] Jaiswal, H., Lindqvist, A.: 'Bystander communication and cell cycle decisions after DNA damage', *Front. Genet.*, 2015, **6**, (1), pp. 63–68

[45] Ojima, M., Furutani, A., Ban, N., *et al.*: 'Persistence of DNA double-strand breaks in normal human cells induced by radiation-induced bystander effect', *Radiat. Res.*, 2010, **175**, (1), pp. 90–96

© The Institution of Engineering and Technology 2019

[46] Geva-Zatorsky, N., Rosenfeld, N., Itzkovitz, S., *et al.*: 'Oscillations and variability in the p53 system', *Mol. Syst. Biol.*, 2006, **2**, (1), pp. 1–13
[47] Mothersill, C., Bucking, C., Smith, R., *et al.*: 'Communication of radiation-induced stress or bystander signals between fish *in vivo*', *Environ. Sci. Technol.*, 2006, **40**, (21), pp. 6859–6864
[48] Rothkamm, K., Löbrich, M..: 'Evidence for a lack of DNA double-strand break repair in human cells exposed to very low X-ray doses', *Proc. Natl. Acad. Sci.*, 2003, **100**, (9), pp. 5057–5062
[49] Richter, M., Dayaram, T., Gilmartin, A., *et al.*: 'WIP1 phosphatase as a potential therapeutic target in neuroblastoma', *PLOS One*, 2015, **10**, (2), p. e0115635
[50] Kononczuk, J., Czyzewska, U., Moczydlowska, J., *et al.*: 'Proline oxidase (POX) as a target for cancer therapy', *Curr. Drug Targets*, 2015, **16**, (13), pp. 1464–1469
[51] Oh, E., Park, H.: 'Implications of NQO1 in cancer therapy', *BMB Rep.*, 2015, **48**, (11), p. 609
[52] Lee, H., Parkinson, E., Granchi, C., *et al.*: 'Reactive oxygen species synergize to potently and selectively induce cancer cell death', *ACS Chem. Biol.*, 2017, **12**, (5), pp. 1416–1424

© The Institution of Engineering and Technology 2019